Simulation of Composite Suction Foundation to Topography Change

San-Shan Lin[#1], Hsing-Yu Wang[#2], Yun-Chih Chiang[*3], Hui-Ming Fang[#4], Sung-Shan Hsiao[#5]

[#] *Department of Harbor and River Engineering, National Taiwan Ocean University*
No.2, Beining Rd., Jhongjheng District, Keelung City 202, Taiwan (R.O.C)

[1]sslin46@gmail.com

[2]hywang1108@gmail.com

[4]hmfang@email.ntou.edu.tw

[5]sshsiao@mail.ntou.edu.tw

[*] *General Education Center, Tzu Chu University*
No.701, Sec. 3, Zhongyang Rd. Hualien 97004, Taiwan (R.O.C)

[3]ycchiang@mail.tcu.edu.tw

The objective of this study was to adequately examine potential wave fields, flow fields, and coastal geomorphological changes in an ocean near an offshore wind farm after installation of a wind power-generating set. The simulation results revealed that geomorphological changes (i.e., scouring and silting variations), from a macroscopic perspective, the installation of the wind turbines did not sufficiently affect the geomorphology of the study area. But a microscopic perspective, changes in the seabed geomorphology were only limited to areas surrounding the submerged piles after the installation of the wind turbines.

***Keywords*—Offshore wind turbines; Composite suction foundation; Numerical model**

I. INTRODUCTION

Over the past 10 year, Taiwan has been actively developing terrestrial wind farms. Currently, a total of 24 wind farms have been established on the island. However, favorable locations for developing wind farms has been exhausted, and wind turbine generators cause considerable noise engendered by wind shear; therefore, establishing offshore wind farms will become a future trend for Taiwan. But the layout of offshore structures is closely related to sedimentation and sedimentation. Because the layout of engineering structures will change the sediment bed dynamic conditions of the original flow field and wave field. Thus, hydraulic analyses are required to prevent offshore wind generators from affecting the ocean environment. For offshore wind power research, [1], [2], [3] and [4] study has been performed on the occurrence and prevention of erosion holes (scour) around mono pile foundations of offshore wind turbines on sandy soils. [5] developed a coupled model to investigate the dynamic interaction between an offshore pile, poroelastic seabed and sea water. [6] analysis and interpretation of monitoring data for the seabed bathymetry local to offshore windfarm foundations has shown how the scour develops in time and highlighted variations between sites with different seabed sediment characteristics, i.e. sands and clays. [7] presented a numerical model for the simulations of the morphological changes in large coastal area and local seabed evolutions near turbine foundation, and an assessment of the possible long-term morphological evolution. Accordingly, this study used the composite suction foundation, and simulated coastal geomorphological changes occurring after the installation of wind turbines at an offshore wind farm located between Zhuwei Fishing Harbor and south of Datan Power Plant. Numerical modeling was performed to examine the influence of the offshore wind power-generating set on its neighboring ocean environment. The results can serve as a reference for subsequent engineering construction activities and long-term geomorphological change analysis.

II. NUMERICAL MODEL

A. Wave Model

The wave model is governed by Boussinesq Equations which were recommended by [8] and incorporates the effect of bottom friction, lateral mixing term and the mechanics of broken spread renewable wave suggested by [9]. The equations are given as:

$$\frac{\partial \eta}{\partial t}+\nabla\left[\left(h+\eta\right)u_a\right]+\nabla\left\{\left(\frac{z_a^2}{2}-\frac{h^2}{6}\right)h\nabla\left(\nabla\cdot u_a\right)+\left(z_a+\frac{h}{2}\right)h\nabla\left[\nabla\left(hu_a\right)\right]\right\}=0 \tag{1}$$

$$\frac{\partial \eta}{\partial t}+\nabla\left[\left(h+\eta\right)u_a\right]+\nabla\left\{\left(\frac{z_a^2}{2}-\frac{h^2}{6}\right)h\nabla\left(\nabla\cdot u_a\right)+\left(z_a+\frac{h}{2}\right)h\nabla\left[\nabla\left(hu_a\right)\right]\right\}=0 \tag{2}$$

In the equations above, formula coordinates function $x=\left(x,y\right)$ is for the horizontal direction coordinates, z is the vertical direction coordinate, t is time, and ∇ is defined as $\left(\partial/\partial x,\partial/\partial y\right)$, $u_a=\left(u,v\right)$ for the water depth, $z=z_a$ is the water particle velocity. R_f , R_b and R_s are respectively

bottom friction, surf correction, and lateral mixing. Their expressed as follows mathematical forms are:

$$R_f = \frac{K}{h+\eta} u_a |u_a| \tag{3}$$

Where K is the friction coefficient, R_b includes two components $\left(R_{bx}, R_{by}\right)$ in x and y directions:

$$R_{bx} = \frac{1}{h+\eta}\{[\nu((h+\eta)u_\alpha)_x]_x + \frac{1}{2}[\nu((h+\eta)u_\alpha)_y + \nu((h+\eta)v_\alpha)_x]_y\} \tag{4}$$

$$R_{bx} = \frac{1}{h+\eta}\{[\nu((h+\eta)u_\alpha)_x]_x + \frac{1}{2}[\nu((h+\eta)u_\alpha)_y + \nu((h+\eta)v_\alpha)_x]_y\} \tag{5}$$

The definition of ν is:

$$\nu = B\delta_b^2 (h+\eta)\eta_t \tag{6}$$

δ_b is the mixing length and chosen to be 1.2, B is a parameter and the expressions proposed by [2] are used:

$$B = \begin{cases} 1, & \eta_t \geq 2\eta_t^* \\ \dfrac{\eta_t}{\eta_t^*} - 1, & \eta_t^* < \eta_t \leq 2\eta_t^* \\ 0, & \eta_t \leq \eta_t^* \end{cases} \tag{7}$$

Therefore, the surf zone water level function can be expressed as:

$$\eta_t^* = \begin{cases} \eta_t^{(F)}, & t - t_0 > T^* \\ \eta_t^{(I)} + \dfrac{t-t_0}{T^*}(\eta_t^{(F)} - \eta_t^{(I)}), & 0 \leq t - t_0 < T^* \end{cases} \tag{8}$$

$$\eta_t^{(I)} = 0.65\sqrt{gh}\ ,\ \eta_t^{(F)} = 0.15\sqrt{gh}\ ,\ \eta_t^{(F)} = 0.15\sqrt{gh} \tag{9}$$

T^* is for passing time, t_0 is for wave breaking time, while $t - t_0$ is for the duration of the surf. Subgrid lateral the mixed terms $R_s = \left(R_{sx}, R_{sy}\right)$ can be expressed as:

$$R_{sx} = \frac{1}{h+\eta}\{[\nu_s((h+\eta)u_\alpha)_x]_x + \frac{1}{2}[\nu_s((h+\eta)u_\alpha)_y + \nu_s((h+\eta)v_\alpha)_x]_y\} \tag{10}$$

$$R_{sy} = \frac{1}{h+\eta}\{[\nu_s((h+\eta)v_\alpha)_y]_y + \frac{1}{2}[\nu_s((h+\eta)u_\alpha)_y + \nu_s((h+\eta)v_\alpha)_x]_x\} \tag{11}$$

ν_s is the viscosity items generated by the subgrid trubulence.

B. Hydraulic Model

The system as follows:

$$\frac{\partial \eta}{\partial t} + \frac{\partial}{\partial x}\left[U\left(h+\eta\right)\right] + \frac{\partial}{\partial y}\left[V\left(h+\eta\right)\right] = 0 \tag{12}$$

$$\frac{\partial U}{\partial t} + U\frac{\partial U}{\partial x} + V\frac{\partial U}{\partial y} = fV - g\frac{\partial \eta}{\partial x} + \frac{1}{\rho}\left(\frac{\partial \tau_{xx}}{\partial x} + \frac{\partial \tau_{yx}}{\partial y}\right) + \frac{1}{\rho\left(h+\eta\right)}\left(\tau_{sx} - \tau_{bx}\right) - \frac{1}{\rho\left(h+\eta\right)}\left(\frac{\partial S_{xx}}{\partial x} + \frac{\partial S_{yx}}{\partial y}\right) \tag{13}$$

$$\frac{\partial V}{\partial t} + U\frac{\partial V}{\partial x} + V\frac{\partial V}{\partial y} = fV - g\frac{\partial \eta}{\partial y} + \frac{1}{\rho}\left(\frac{\partial \tau_{xy}}{\partial x} + \frac{\partial \tau_{yy}}{\partial y}\right) + \frac{1}{\rho\left(h+\eta\right)}\left(\tau_{sy} - \tau_{by}\right) - \frac{1}{\rho\left(h+\eta\right)}\left(\frac{\partial S_{xy}}{\partial x} + \frac{\partial S_{yy}}{\partial y}\right) \tag{14}$$

U and V is the velocity component of the flow field in the x and y directions, t represents time, η is the fluid dynamic pressure, and S_{ij} is the wave field calculation result obtained from the radiation stress.

Considering the three-dimensional coordinate system shown in Figure 1, wherein Y is the coast direction, X is the onshore and offshore direction, and Z is the vertical direction of the water depth. Assuming that the water depth of the vertical direction of the flow rate is much smaller than the horizontal direction of the flow rate, the momentum equation is:

$$\frac{\partial u}{\partial t} = -\frac{1}{\rho}\frac{\partial p}{\partial x} + \frac{\partial}{\partial z}\left(\nu_t \frac{\partial u}{\partial z}\right) + \frac{1}{\rho}\frac{\partial \overline{\tau^x}}{\partial z} \tag{15}$$

$$\frac{\partial u}{\partial t} = -\frac{1}{\rho}\frac{\partial p}{\partial x} + \frac{\partial}{\partial z}\left(\nu_t \frac{\partial u}{\partial z}\right) + \frac{1}{\rho}\frac{\partial \overline{\tau^x}}{\partial z} \tag{16}$$

p is the water pressure, ν_t is the eddy viscosity coefficient, $\overline{\tau^x}$ and $\overline{\tau^y}$ are the shear stress though the X , Y directions.

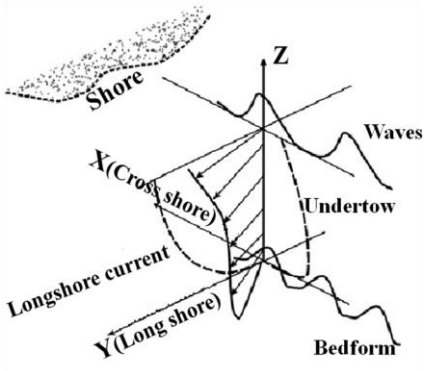

Fig 1. the coordination of the Q-3D hydrodynamic system

Formula (15) and (16) both ignores the convection terms. It is mainly because that 2HD hydrodynamic flow field pattern already covers the convective term effects of the horizontal distribution. The 1DV shear stress items in this article take proposal from [10] and [11]. Thus, the shear stress distribution in a water depth of the vertical direction can be analyzed by using the vertical force balance in the surf zone. The shear stress should include: shear stress caused by the wave transfer process, by the surf, by the stress of the bottom boundary layer friction effect and by the water level change due to equilibrium radiation. Detailed theoretical explanations is like what [12] shown. Referenced from [13], Eddy viscosity coefficient can be divided into three parts which are the wave at the bottom of the oscillation, periodic average velocity items and broken wave effect term. This article adopts the one-equation k-closure turbulence model:

$$\frac{\partial k}{\partial t}=\frac{\partial}{\partial z}\left(\frac{\nu_{tb}}{\sigma_k}\frac{\partial k}{\partial z}\right)+\nu_{tb}\left[\left(\frac{\partial u}{\partial z}\right)^2+\left(\frac{\partial v}{\partial z}\right)^2\right]+\frac{P_r}{\rho}-\varepsilon \tag{17}$$

$\sigma_k=1.0$ is the constant turbulent flow energy, and P_r is the turbulence power on the surface caused by the breaking waves.

$$\varepsilon=c_1k^{3/2}/l \tag{18}$$

The turbulence length is suggested by [10]:

$$l=\begin{cases}c_1^{1/4}\kappa z & ,z\le l_{\max}/\left(\kappa c_1^{1/4}\right)\\ l_{\max} & ,z>l_{\max}/\left(\kappa c_1^{1/4}\right)\end{cases} \tag{19}$$

$l_{\max}=0.1h,\quad c_1=0.09$

The suggested calculation from [10]:

$$P_r=\alpha_p\mathrm{DISS} \tag{20}$$

The constatnts $\alpha_p=0.33$, and the energy dissipated item DISS is from [14]:

$$\mathrm{DISS}=\rho g c\delta_r\tan\phi_0 \tag{21}$$

c is the wave velocity, φ_0 is the broken wave surface which initially assumed to be 10 degrees; δ_r is the thickness of the surface waves:

$$\delta_r=\frac{2\left(h+H/2\right)}{L} \tag{22}$$

C. Sediment Transport Model

1) Bed Load Sediment Transport

Improved the Bedload formula from [12] and [15], the introduction of the nearshore waves to shore transfer process asymmetry effect are added to establish the mode of calculating the amount of drift sand:

$$q_b=\overline{\Phi}_b\left[g\left(s-1\right)d_{50}^3\right]^{1/2} \tag{23}$$

$$\overline{\Phi}_b=\left(\overline{\Phi}_{bx}^2+\overline{\Phi}_{by}^2\right)^{1/2} \tag{24}$$

$$\overline{\Phi}_{bx}=11\left[t_c\left(\theta_{cx}-\theta_c\right)^{1.65}-t_t\left(\theta_{tx}-\theta_c\right)^{1.65}\right] \tag{25}$$

$$\overline{\Phi}_{by}=11\left(\theta_y-\theta_c\right)^{1.65}$$

In the four equations above, g is the gravitational acceleration, s is the relative density ($s=\rho_s/\rho$, ρ_s is the density of sand) , d_{50} is the median particle, Φ_{bis} dimensionless drift sand transfer rate. The subscripts, x and y are the transmission direction and the vertical direction. The half cycle of crest role and trough role, the vertical wave direction of Shears shear stress coefficient are from [8] and [13]:

$$\theta_{cx}=\frac{1}{2}\frac{\left(f_{cw}\right)_{cx}u_{cx}^2}{\left(s-1\right)gd_{50}} \tag{26}$$

$$\theta_{tx}=\frac{1}{2}\frac{\left(f_{cw}\right)_{tx}u_{tx}^2}{\left(s-1\right)gd_{50}} \tag{27}$$

$$\theta_y=\frac{1}{2}\frac{f_cU_0^2\sin^2\left(\phi\right)}{\left(s-1\right)gd_{50}} \tag{28}$$

f_{cw} is the friction coefficient under the action of wave current while u_{cx} and u_{tx} are the equivalent peaks and troughs of a half cycle.

2) Suspended Load Sediment Transport

The calculation of suspended load is adopted from [12] and [15], which coordinated with the three-dimensional flow field:

$$\frac{\partial C}{\partial t}=w_s\frac{\partial C}{\partial z}+\frac{\partial}{\partial z}\left(\varepsilon_{sd}\frac{\partial C}{\partial z}\right) \tag{29}$$

w_s is the settling velocity in [16], ε_{sd} is the turbulent eddy viscosity coefficient in [17].

After obtained the concentration of pseudo three-dimensional flow field and suspended drift sand, the water depth can be use to get the instantaneous drift sand trasnfer rate:

$$q_s=\int_{za}^{h}\bar{c}\left(z\right)\bar{u}\left(z\right)dz \tag{30}$$

z_a is the referent height, assumed as 2.5mm in [16] and h is the water depth.

III. Analysis of the Interaction between Sea States and Wind Turbine Structures

1) Simulations set-up

The simulation area (Fig. 2) is between Zhuwei Fishing Harbor and south of Datan Power Plant, which is 22.5 km long in the alongshore direction and 12.0 km wide in the on-off shore direction with a maximum depth of around 50.0 m. This study employed the wave and tidal current data to construct a numerical model for coastal geomorphological change analysis. The modules used in the simulation analysis are presented in Figure 3 Specifically, variations in wave flow fields induce changes in the quantity and direction of drifting sand grains. Changes in the distribution of drifting sand grains can subsequently lead to scouring and silting variations along the coast. Such changes can then, in turn, recurrently affect the condition of wave flow fields. Table 1 lists wave data collected in "The Plan of Coastal Monitoring and Investigation for Taoyuan, Hsinchu and Miaoli County" wave conditions obtained from the numerical simulation; both sets of data could be applied to derive the required offshore wave data to be used as the input for the subsequent simulation. There are three durations of morphological simulation in one year. They are the duration of summer monsoon, the duration of typhoon, and the duration of winter monsoon. During monsoon period, the flow field is added by waves driven currents and tidal period averaged currents. In the duration of typhoon, the typhoon waves condition, storm surge water-level, and characteristic flood discharge are employed. The spatial grid sizes of $\Delta x=\Delta y=15m$ are used in all models (including the sub-models for waves and currents). The time step interval of $\Delta t=1s$ is used for the nearshore current sub-model and $\Delta t=60s$ for the morphological model.

Fig. 1 The simulation area

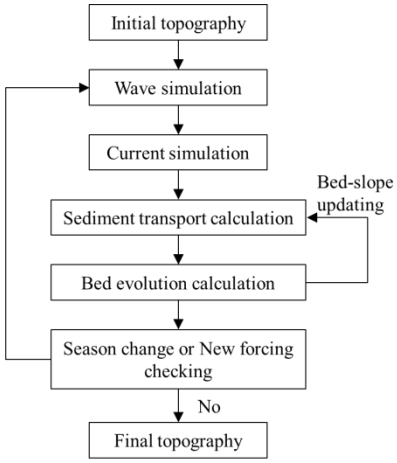

Fig. 2 Flow chart of the coastal morphological modeling

TABLE I
INPUT DATA FOR NUMERICAL SIMULATION

Stage	Duration	Simulation wave conditions
Summer monsoon	150 days	NNW, H=0.5m, T=4.6s
Typhoon	10 days	NNE, H=9.3m, T=12.8s
Winter monsoon	210 days	NNW, H=1.4m, T=6.0s

2) Model analysis

The wave fields of summer monsoon, winter monsoon and typhoon are shown in Figures 3-5. The current fields of wave-driven currents during different monsoon are shown in Figures 6-11. Figure 12 illustrates the simulation results obtained in the study area, revealing more noticeable geomorphological changes in the shallow inshore area than in the deep offshore area. These results are consistent with the relatively noticeable real-world changes in the activity of drifting sand in the shallow inshore area. These results essentially indicate that the shallow inshore area (particularly the area surrounding coastal structures, such as the reclaimed land close to sea walls) exhibited geomorphological changes as indicated by its scouring and silting variations. According to the results derived from the real-time simulation of coastal geomorphological changes under 50-year recurrent typhoon-induced wave conditions, the shallow inshore area exhibited more noticeable scouring and silting variations and geomorphological changes, particularly in regions surrounding coastal structures, than did the deep offshore area (the studied wind farm). However, the scouring and silting range of typhoon-induced waves in the shallow inshore area was slightly broader than that in the monsoon season, suggesting that typhoon-driven waves also influenced the deep offshore area. Because the offshore wind farm was located in an area with a greater water depth than other areas, no considerable morphemically changes were detected around the farm under the 50-year recurrent typhoon-induced wave conditions.

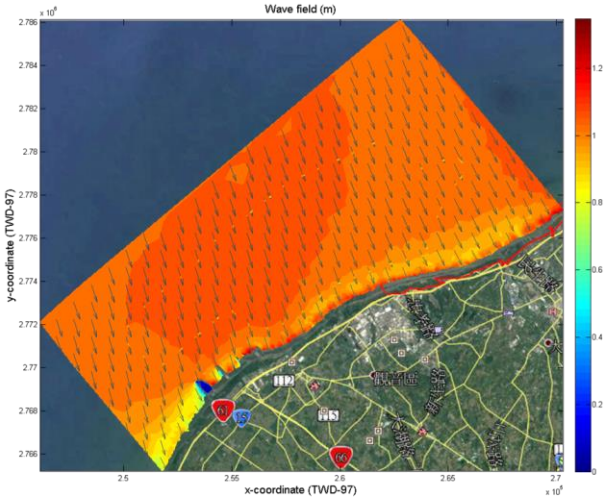

Fig. 3 Wave field during summer monsoon

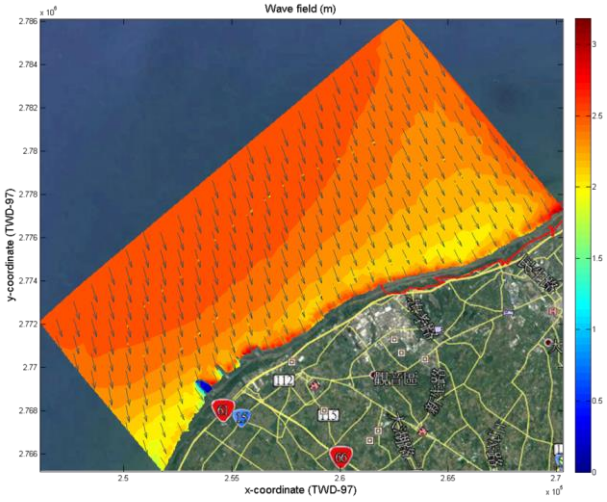

Fig. 4 Wave field during winter monsoon

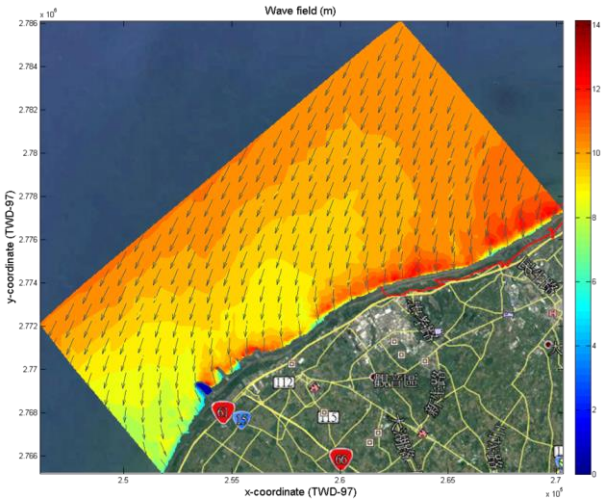

Fig. 5 Wave field during typhoon

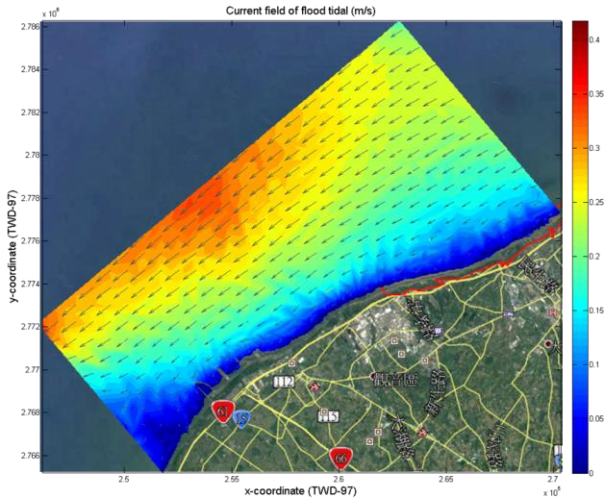

Fig. 6 Current field of flood tidal during summer monsoon

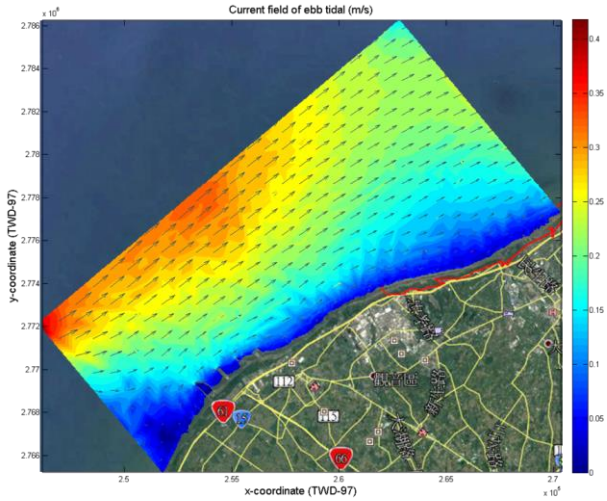

Fig. 7 Current field of ebb tidal during summer monsoon

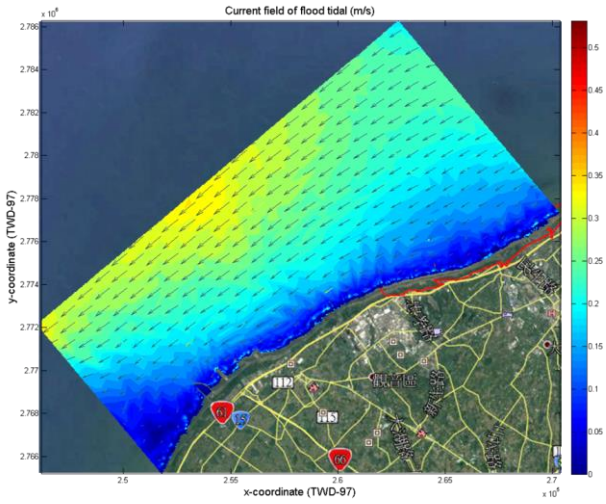

Fig. 8 Current field of flood tidal during winter monsoon

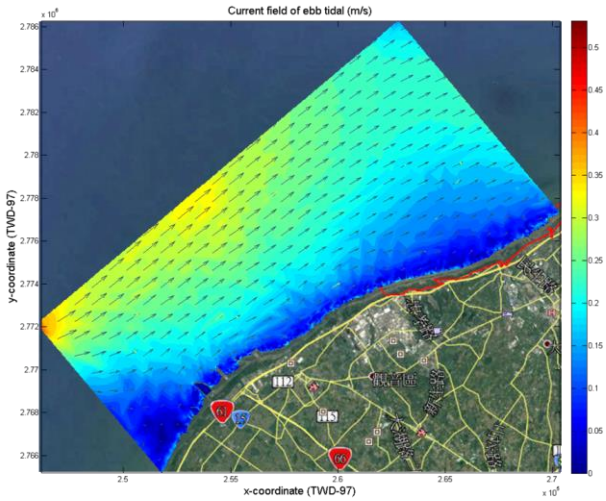

Fig. 9 Current field of ebb tidal during winter monsoon

Fig. 10 Current field of flood tidal during typhoon

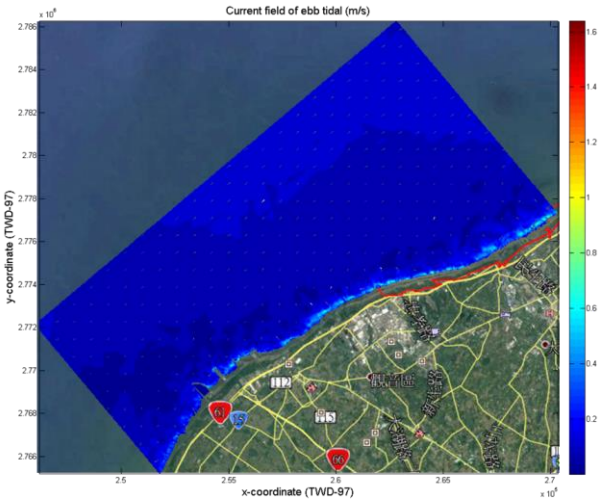

Fig. 11 Current field of ebb tidal during typhoon

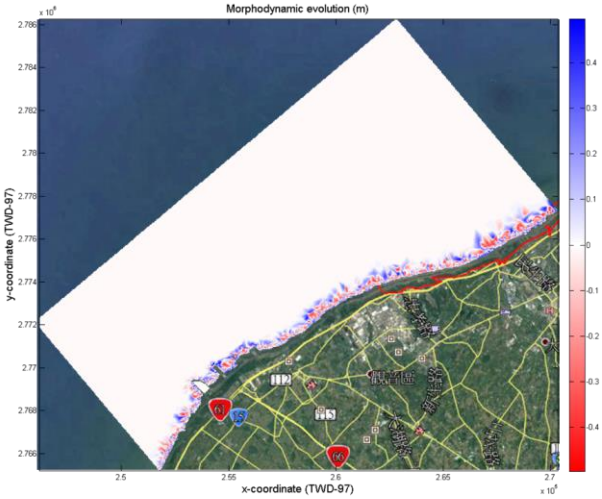

Fig. 12 Morphodynamic evolution after one year

3) Results and Analysis

The offshore wind turbines examined in this study were constructed on a composite suction foundation, as shown in Figure 13. According to water wave theory, a circular cylinder with a diameter more than one-twentieth of the wavelength does generate substantial diffraction or scattering. In this study, the wave and flow field simulation results obtained after the installation of the wind turbines in the offshore area near the wind farm were compared with the wave and flow field simulation results obtained without the installation of offshore wind turbines. The comparison results revealed that the installation of the offshore wind turbines may effects on exogenic geomorphic agents (i.e., ocean waves and flows) reflect the actual geomorphological changes in the study area after the wind turbine installation (Figures 14–22). But the interval between the wind turbines considerably exceeded the actual range of influence of scouring and silting near the piles. The simulation results (Figure 23) indicated that erosion (or scouring) primarily occurred on the seabed on the upstream side of the piles, whose front edges directly faced the impact of waves; by contrast, silting primarily occurred on the seabed on the downstream side of the piles, particularly in areas along the direction of typhoon-induced waves. This finding sufficiently supports the aforementioned statement that the range of influence of waves was limited to areas surrounding the submerged piles.

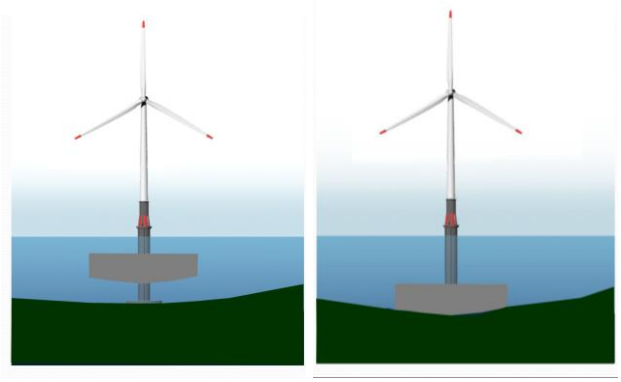

Fig. 13 Composite suction foundation from [18]

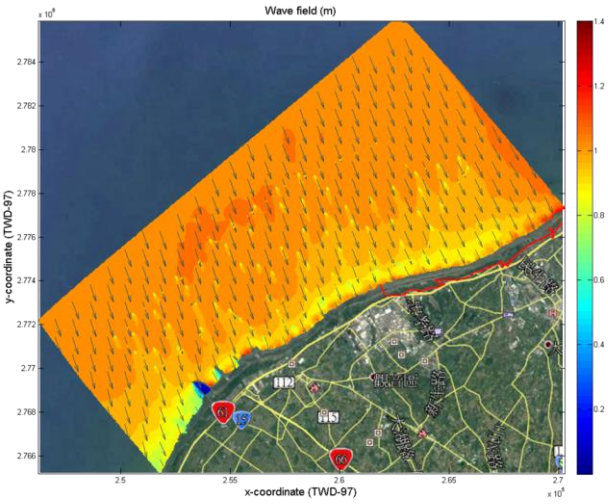

Fig. 14 Wave field during summer monsoon after set up the wind turbine

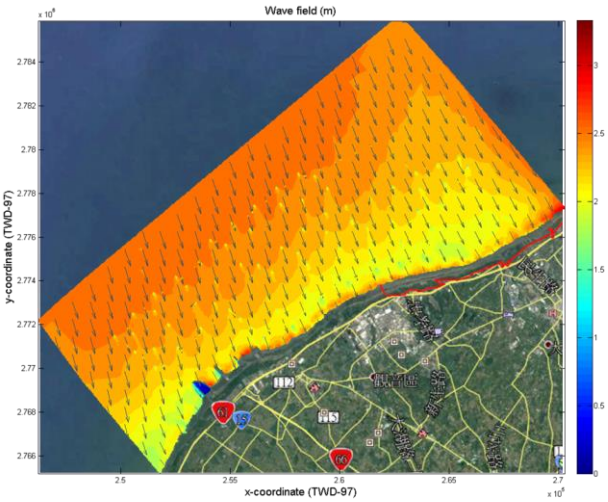

Fig. 15 Wave field during winter monsoon after set up the wind turbine

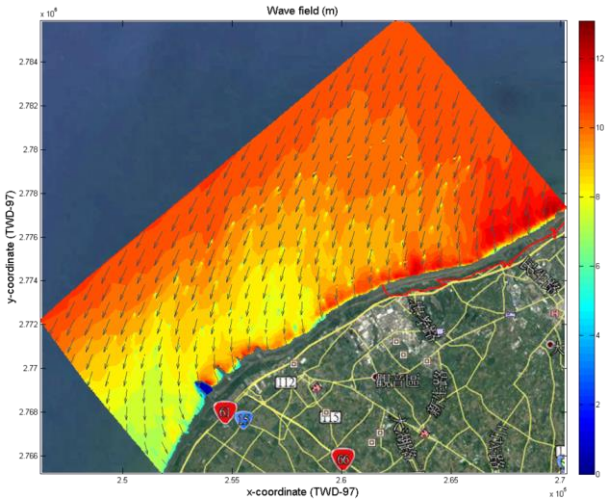

Fig. 16 Wave field during typhoon after set up the wind turbine

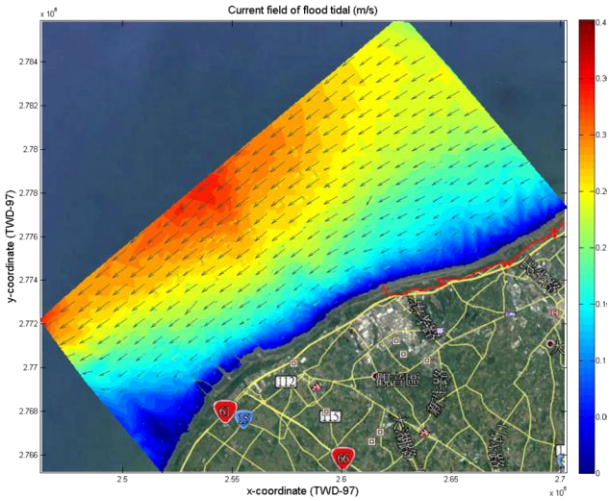

Fig. 17 Current field of flood tidal during summer monsoon after set up the wind turbine

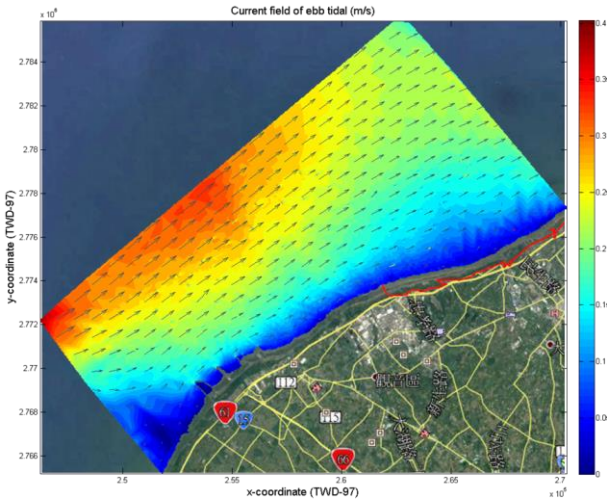

Fig. 18 Current field of ebb tidal during summer monsoon after set up the wind turbine

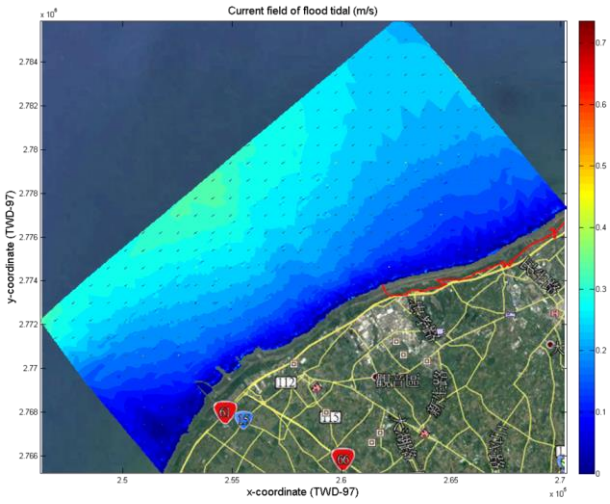

Fig. 19 Current field of flood tidal during winter monsoon after set up the wind turbine

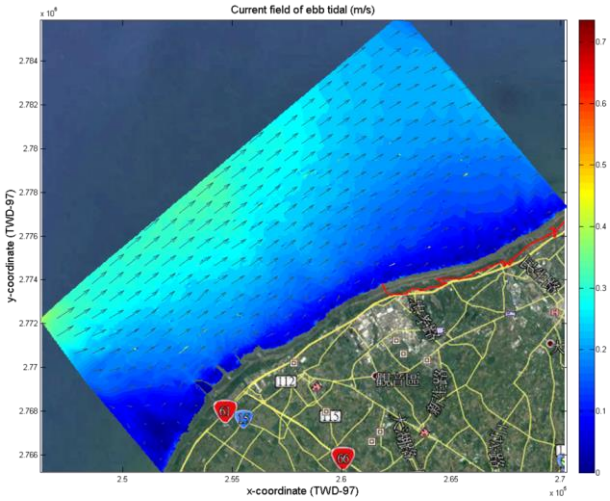

Fig. 20 Current field of ebb tidal during winter monsoon after set up the wind turbine

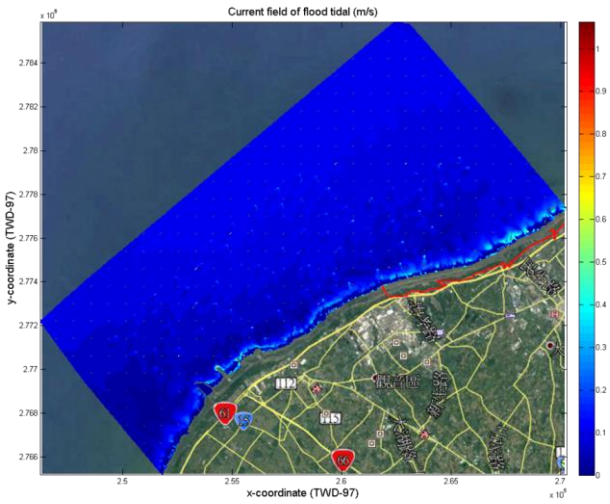

Fig. 21 Current field of flood tidal during typhoon after set up the wind turbine

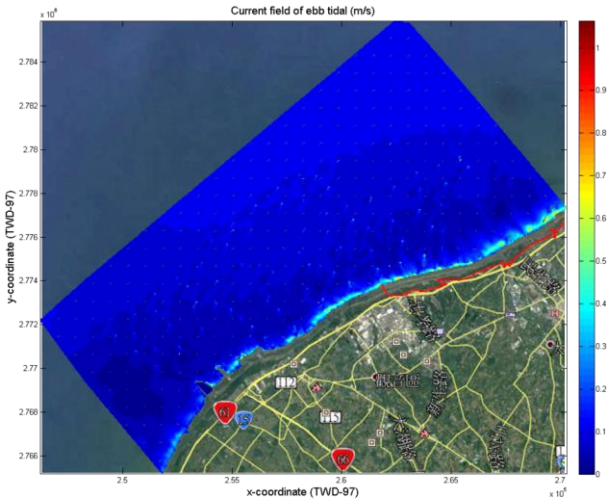

Fig. 22 Current field of ebb tidal during typhoon after set up the wind turbine

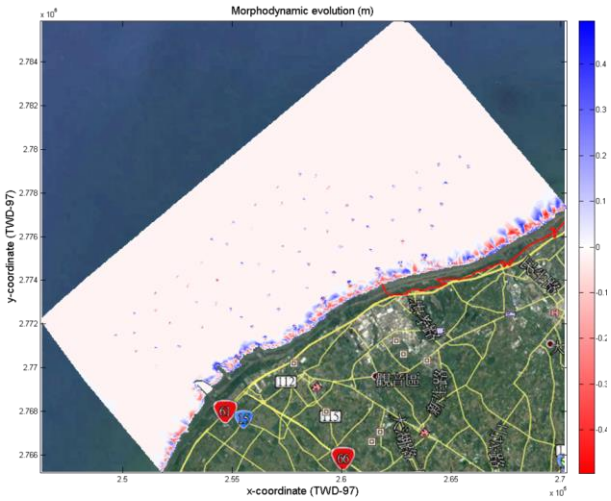

Fig. 23 Morphodynamic evolution after one year after set up the wind turbine

IV. Conclusions

Under monsoon and typhoon conditions, geomorphological changes in the study area were mostly observed in the shallow inshore area, particularly in regions surrounding coastal structures. From a macroscopic perspective, the installation of the wind turbines did not sufficiently affect the geomorphology of the study area. And a microscopic perspective, changes in the seabed geomorphology were only limited to areas surrounding the submerged piles after the installation of the wind turbines. The effects of the typhoon conditions engendered greater degrees of scouring and silting variations, compared with the effects of the monsoon conditions, resulting in higher degrees of scouring and silting variations in the deep offshore area than in the shallow inshore area. For the several wind turbines and their piles in the deep offshore area, the most notable geomorphological change was the variation in the characteristics of the local scour and silt. The analysis results can serve as references for the future planning and design of protective mechanisms against scouring and silting around pile structures supporting offshore wind turbines.

References

[1] J. H. Den Boon, J. Sutherland, R. Whitehouse, R. Soulsby, C. J. M. Stam, K. Verhoeven, M. Høgedal, and T. Hald, "Scour behaviour and scour protection for monopile foundations of offshore wind turbines," Proceedings of the European Wind Energy Conference, Vol. 14, 2004.

[2] R. J. S. Whitehouse, J. Sutherland, and D. O'Brien, "Seabed scour assessment for offshore windfarm," Proceedings of the 3rd International Conference on Scour and Erosion, 1-22, 2006.

[3] E. A. Hansen, H. J. Simonsen, A. W. Nielsen, J. Pedersen, and M. Høgedal, "Scour protection around offshore wind turbine foundations, full-scale measurements," Scientific Proceedings of the European Wind Energy Conference, Vol. 2007, 132-138, 2007.

[4] R. Y. Yang, H. H. Chen, H. H. Hwung, W. P. Jiang, and N. T. Wu, "Experimental study on the loading and scour of the Jacket type offshore wind turbine foundation," Coastal Engineering Proceedings, 1(32), 25, 2011.

[5] J. F. Lu, and D. S. Jeng, "A Coupled Model for an Offshore Pile, Seabed and Seawater Interaction," Journal of Coastal Research, 389-393, 2007.

[6] R. J. S. Whitehouse, J. M. Harris, J. Sutherland, and J. Rees, "The nature of scour development and scour protection at offshore windfarm foundations," Marine Pollution Bulletin, 62(1), 73-88, 2011.

[7] Y. C. Chiang, S. S. Hsiao, H. M. Fang, H. Y. Wang, and M. C. Lin, "Numerical of morphological changes around offshore wind turbine foundations in Taiwan western coast," Proceedings of the Twenty-fourth (2014) International Ocean and Polar Engineering Conference, 227-233, 2014.

[8] Y. C. Chiang, "Numerical modelling for coastal morphodynamic evolutions," National Taiwan University Doctor Thesis, 2009.

[9] A. B. Kennedy, Q. Chen, J. T. Kirby, and R. A Dalrymple, "Boussinesq modelling of wave transformation, breaking, and runup. I: 1D," J. Waterway Port Coastal Ocean Engineering, Vol. 126, pp. 39-47, 2000.

[10] R. Deigaard, P. Justesen, and J. Fredsøe, "Modelling of undertow by a one-equation turbulence model," Coastal Engineering, Vol. 15, 5-6, pp. 431-458, 1991.

[11] R. Deigaard, "A note on the three- dimensional shear stress distribution in a surf zone," Coastal Engineering, Vol. 20, 1-2, pp. 157-171, 1993.

[12] M. C. Lin, Y. C. Chiang, and S. S. Hsiao, "A study of the sediment transport formula under combined Wave and current conditions," J. of Coastal and Ocean Engineering, Vol. 9, No. 2, pp. 177-205, 2009.

[13] I. Brøker Hedegaard, R. Deigaard, and J. Fredsøe, "Onshore/Offshore sediment transport and morphological modelling of coastal profiles," Coastal Sediments, Vol. 1, pp. 643-657, 1991.

[14] R. Deigaard, "Mathematical modeling of waves in surf zone," ISVA (Inst. of Hydrodynamics and Hydraulic Engineering), Tech. Univ. of Denmark, Progress rep. No. 69, pp. 47-59, 1989.

[15] Y. C. Chiang, S. S. Hsiao, M. C. Lin, and W. H. Hsu, "Numerical simulations of offshore sandbar formation," Proceedings of the 33rd Ocean Engineering Conference in Taiwan, pp. 411-416, 2011.

[16] R. L. Soulsby, "Dynamics of marine sands," Thomas Telford Publications, London, 1997.

[17] J. Fredsøe and R. Deigaard, "Mechanics of Coastal Sediment Transport," Advanced Series in Ocean Eng., 3, World Scientific, p. 369, 1992.

[18] S. S. Lin, Y. C. Chiang, X. H. Lin, H. Y. Wang, and S. S. Hsiao, Numerical Studies on Performance of Offshore Wind Turbine Composite Suction Pile in Sand Subjected to Combined Loading, *Geotechnical Engineering Journal of the SEAGS & AGSSEA*, Vol. 48, No. 4, 2017.